Applied Physics Express **8**, 093002 (2015)
http://dx.doi.org/**10.7567/APEX.8.093002**

Nanopatterning of magnetic domains: Fe coverage of self-assembled alumina nanostructure

Chii-Bin Wu[1]*, Bo-Yao Wang[2], Wen-Chin Lin[3], Zheng Gai[4], and Minn-Tsong Lin[5,6]*

[1]*Department of Physics, Chung Yuan Christian University, Chungli 32023, Taiwan*
[2]*Department of Physics, National Changhua University of Education, Changhua 500, Taiwan*
[3]*Department of Physics, National Taiwan Normal University, Taipei 11677, Taiwan*
[4]*Center for Nanophase Materials Science Division, Oak Ridge National Laboratory, Oak Ridge, TN 37831, U.S.A.*
[5]*Department of Physics, National Taiwan University, 10617 Taipei, Taiwan*
[6]*Institute of Atomic and Molecular Sciences, Academia Sinica, 10617 Taipei, Taiwan*
E-mail: chiibinwu@cycu.edu.tw; mtlin@phys.ntu.edu.tw

Received May 17, 2015; accepted July 31, 2015; published online August 19, 2015

Nanosized ultrathin magnetic films were prepared by controlling the deposition of Fe onto an oxidized NiAl(001) surface with an alumina nanostructure on it. Because the ultrathin ferromagnetic Fe films on the bare NiAl(001) surface are separated by paramagnetic Fe nanoparticles on the alumina stripes, as determined by scanning electron microscopy with spin analysis, they form rectangular domains with sizes ranging from tens of nanometer to larger than a micrometer. Magnetic domain patterning can thus be achieved by controlling the Fe coverage and nanostructured template.

Fabrication of magnetic nanostructures has attracted much attention in recent decades, stimulated mainly by advances in magnetic storage technology and their novel properties at small length scales.[1)] Many lithographic approaches and bottom-up self-assembly methods have been reported.[1–10)] However, in the regime of ultrathin films that are several monolayers thick, magnetic nanostructures at room temperature are seldom reported.[11,12)] Here we propose a method of in situ preparation of ultrathin films with magnetic nanopatterns at room temperature in which the pattern size can be tuned from tens of nanometers to larger than a micrometer.

Magnetic nanopatterns can be prepared by depositing an ultrathin ferromagnetic film onto a surface with nanosized heterostructures. It has been well demonstrated that ultrathin single-crystalline alumina layers can be formed on the NiAl(001) surface by sufficient oxygen exposure at around 1000 K in ultrahigh vacuum.[13)] When a very low oxygen dosage is used to oxidize the NiAl(001) crystal, its surface is covered with alumina stripes with widths of nanometers to tens of nanometers and lengths from tens to hundreds of nanometers, depending on the oxidation parameters.[14,15)] Because Fe grows as particles on alumina but as a continuous film on the uncovered NiAl(001) surface, the Fe deposited on such a nanostructured template forms nanosized iron films separated by nanoparticle chains.[16,17)] Furthermore, because the Curie temperature of Fe particles is lower than that of Fe films, the ferromagnetic films are separated by paramagnetic nanoparticle chains at room temperature.[18–20)] The Fe coverage range in this scenario is 2 atomic monolayers (MLs) to 10 MLs. Within this coverage range, the oxygen dosage determines the underlying alumina structure as well as the magnetic domain pattern size, which continuously decreases from larger than a micrometer at 1 L (defined as an oxygen dosage of 1.0×10^{-6} mbar·s) to 100 nanometers at 6 L and finally disappears at 20 L, where the entire sample is covered by paramagnetic nanoparticles. This method enables in situ preparation of ultrathin Fe films having a controllable domain size ranging from tens of nanometers to larger than a micrometer.

The experiment is conducted in an ultrahigh vacuum chamber equipped with surface science analysis tools, such as low-energy electron diffraction (LEED) and Auger electron spectroscopy (AES).[21)] The NiAl(001) substrate is cleaned by a standard sputter annealing procedure.[16)] Next, the substrate is heated to around 1000 K and held at that temperature for 1 h before oxygen exposure. Oxidation is performed by exposing the sample to oxygen ambient with a pressure from 1.0×10^{-8} to 5.0×10^{-8} mbar, depending on the oxidation condition. After oxidation, the sample is held at high temperature for another 1 h and then cooled to room temperature for Fe deposition. Magnetic domain images are taken by the scanning electron microscope with polarization analysis (SEMPA) facilities at the Center for Nanophase Materials Science Division of Oak Ridge National Laboratory. The SEMPA was equipped with a spin-polarized LEED detector, which measured the spin contrast in two orthogonal directions simultaneously during scanning. Thus, the in-plane magnetization vectors at each pixel of a SEMPA image can be determined.

For convenient description, the NiAl(001) sample with an n L oxygen dosage is called an n L alumina sample hereafter. Figure 1(a) shows the LEED pattern of a 10 L alumina sample. Aside from the main body-centered-cubic diffraction spots, there are two additional superstructures. The $c(\sqrt{2} \times 3\sqrt{2})R45^\circ$ superstructure corresponds to the Al-covered NiAl surface after 1000 K annealing.[22)] The $(2 \times 1, 1 \times 2)$ superstructure results from the θ-alumina on the NiAl(001) surface.[13)] The coexistence of these two structures indicates that the NiAl surface is partially covered by the alumina, and the uncovered surface retains the same structure as that with no oxygen dosage. The topography of this sample, shown in Fig. 1(b), is observed by a scanning tunneling microscope (STM) in constant current mode with a scanning direction rotated by 45°. The feedback parameters are a sample bias of +2.5 V and tunneling current of 1.0 nA. The tunneling conductance map of the same area, shown in Fig. 1(c), is taken simultaneously with the topography image under the same feedback parameters using a lock-in technique. Clearly two contrast levels can be identified, corresponding to areas of alumina and uncovered NiAl surface. The tunneling spectra, taken under the feedback parameters of a +2.5 V sample bias and a 1.0 nA tunneling current and averaged over the bright and dark regions in Fig. 1(c), are shown in Fig. 1(d), where the solid (dashed) lines correspond to the bright (dark) areas. The tunneling gap

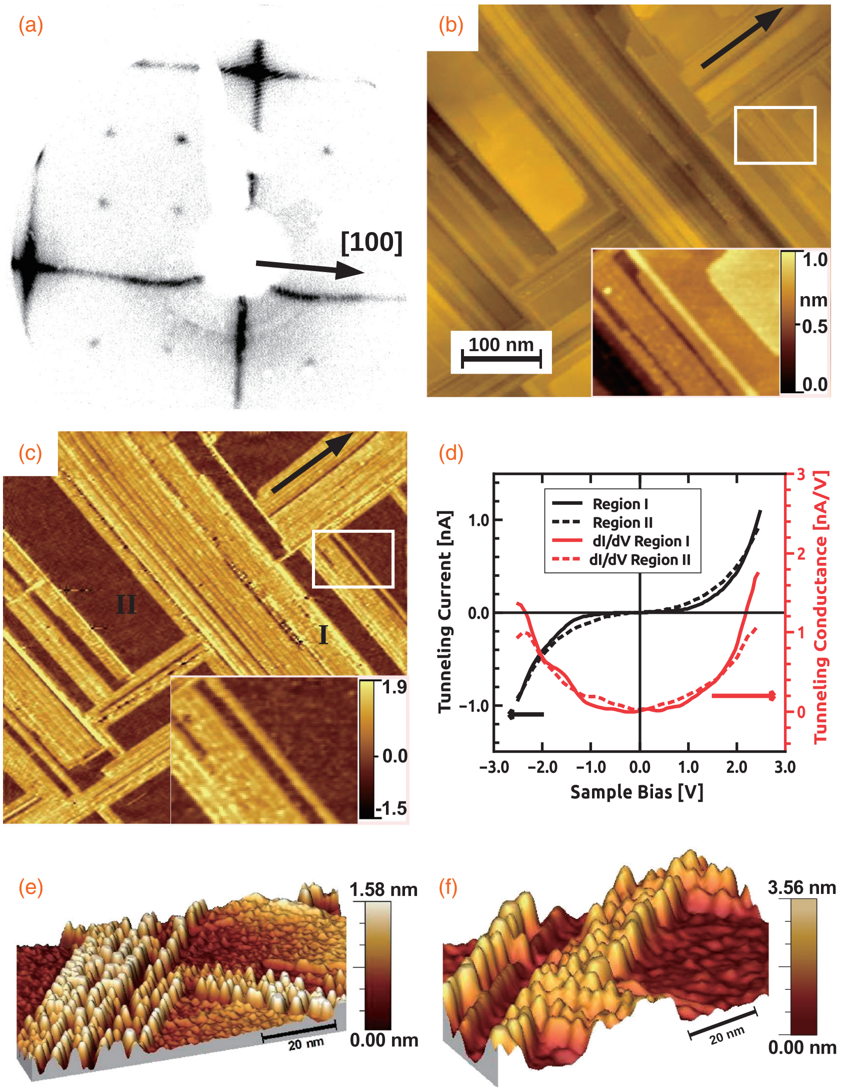

Fig. 1. (a) LEED pattern of 10 L alumina/NiAl(001) at electron energy of 36.3 eV. (b) STM topography image of the same sample, and (c) the corresponding tunneling conductance map of the same area, with a sample bias of +2.5 V and feedback current of 1.0 nA. Arrows indicate the [100] crystalline direction. Insets in (b) and (c) correspond to the areas enclosed by white rectangles. (d) Tunneling spectra and *I*–*V* (black) and numerically derived dI/dV–V (red) characteristics, averaged over alumina (solid line) and NiAl surface (dashed line) and taken with feedback parameters of a +2.5 V sample bias and a 1.0 nA tunneling current. STM topography images of (e) 0.5 ML and (f) 7.5 ML Fe grown on 10 L alumina sample.

of ~2 V (solid line) confirms that the bright area is indeed an insulator-like alumina stripe, consistent with the result reported in Ref. 14. From the conductance map, it is clear that the NiAl surface is partitioned into submicron rectangles by the alumina stripes. After deposition of 0.5 ML of Fe, defined as one atomic layer of Fe(001) surface, onto the surface, well-aligned and separated nanoparticles on alumina stripes can be distinguished from the Fe films, as shown in Fig. 1(e). If the Fe coverage is increased to 7.5 MLs, as shown in Fig. 1(f), the nanoparticles become larger and taller, whereas the films remain at the same corrugation level. Therefore, the individual Fe films are well separated from each other by the nanoparticle chains on alumina stripes at this coverage. With increasing coverage on the surface, one can expect the films to become increasingly connected through the particles and finally become a continuous film on the entire surface.

Figure 2 demonstrates the difference between the magnetic domains on a clean NiAl surface and those on a partially oxidized NiAl surface. Without the alumina, the continuous 7.5 ML Fe film has a domain size larger than 10 µm, as shown in Fig. 2(a). This is consistent with the result in Ref. 23. The histogram of the angle distribution reveals two domains aligned antiparallel to each other with one easy axis pointing to around 170°. However, when the film is deposited onto the surface of a 6 L alumina sample, the domain structure becomes fragmented and consists of many small rectangular stripes with sizes ranging from 100 nm to micrometers. The angular distribution reveals the two orthogonal uniaxial easy axes of the system, with one pointing to around 300°. The easy axis rotation between the continuous and nanopatterned films might be due to the confined geometry in the latter case. Bulk Fe has a magnetic easy axis along the ⟨100⟩ direction, which is parallel to the long axis of the alumina stripes. However, the continuous film shows an easy axis rotated by about 50°. This might be due to the $c\sqrt{2} \times 3\sqrt{2}R45^\circ$ superstructure of the NiAl(001) surface.[22)]

To further demonstrate the evolution of the magnetic domains with the oxygen dosage, 5.0 ML Fe was deposited on 1, 4, and 20 L alumina samples; their domain images are

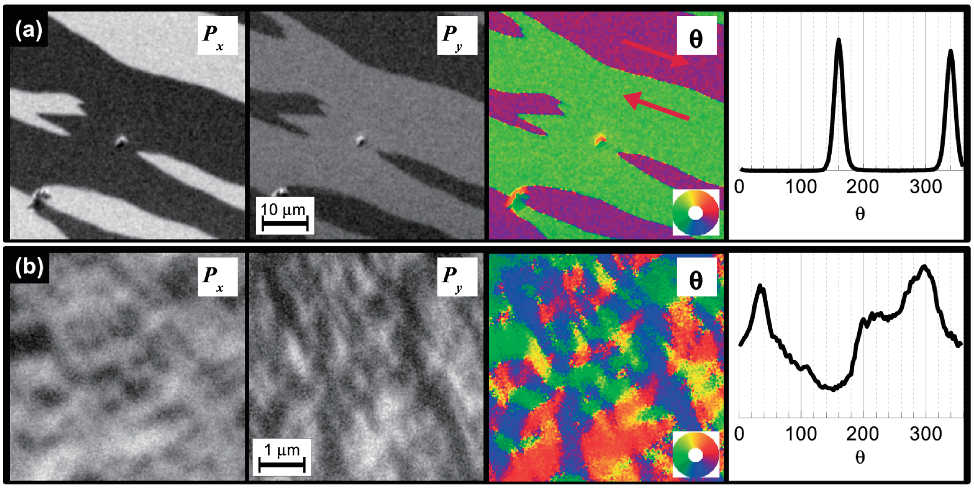

Fig. 2. SEMPA magnetic domain images of 7.5 ML Fe on (a) the NiAl(001) surface and (b) the 6 L alumina/NiAl(001) sample. Arrows in (a) indicate the magnetization directions of the corresponding domains. Rightmost panels are histograms of the angle (θ) maps. Note that the scale bar in (a) is 10 µm, and that in (b) is only 1 µm.

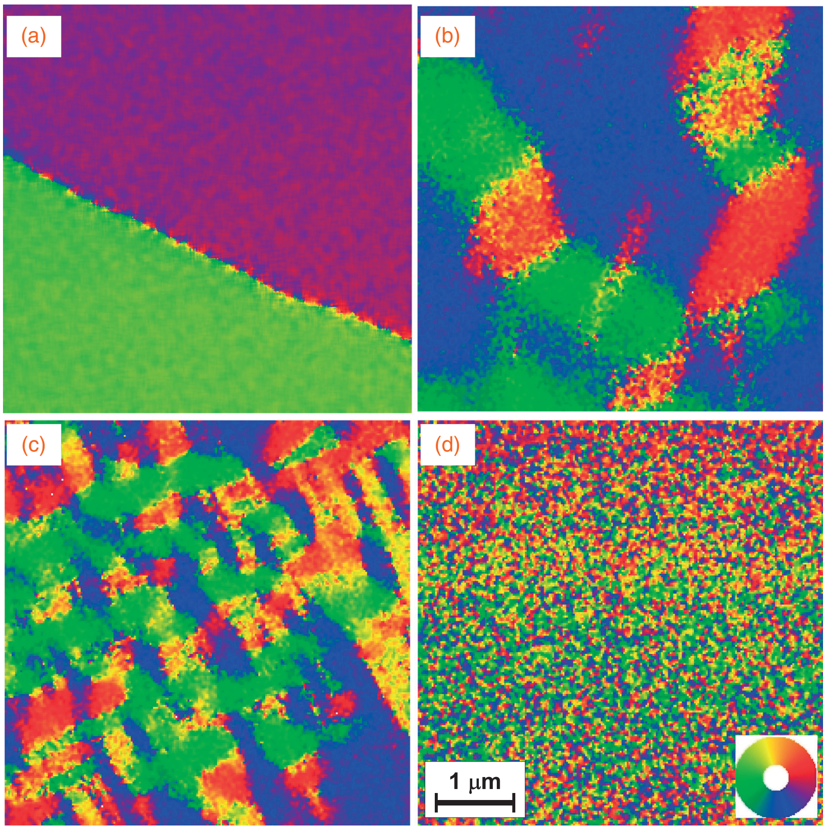

Fig. 3. Magnetic domain image of (a) 7.5 ML Fe on NiAl(001) surface and 5 ML Fe on the (b) 1 L, (c) 4 L, and (d) 20 L alumina samples. Scale bar is the same for all of these images.

shown in Figs. 3(b), 3(c), and 3(d), respectively. For comparison, the domain image of a continuous 7.5 ML Fe film is also shown in Fig. 3(a). In Fig. 3(b), the average domain size is around 1 µm, and the domains are not rectangular. This is because at such a low oxygen dosage, the number of alumina stripes, and thus of nanoparticle chains, is so small that the film is not perfectly partitioned. In Fig. 3(c), the film is perfectly partitioned into rectangles with an average width of around 400 nm and length of about 1 µm. For the 20 L alumina sample, the surface is almost fully covered by alumina layers, and the deposited Fe atoms all exist in particle form. Because the measurement is performed at room temperature, which is higher than the Curie temperature of 5.0 ML Fe nanoparticles, no domain contrast can be observed, and only a noisy background signal exists.

In Fig. 4, we study the effect of the Fe coverage on the domain structure. The domain images are taken at the same location on the sample as the Fe coverage is increased. Figure 4(a) shows a magnetic domain image of 5.0 ML Fe on a 1 L alumina sample. The color code for the magnetization direction is indicated in the color ring in Fig. 4(c). The image is dominated by blue domains, with few green and red areas

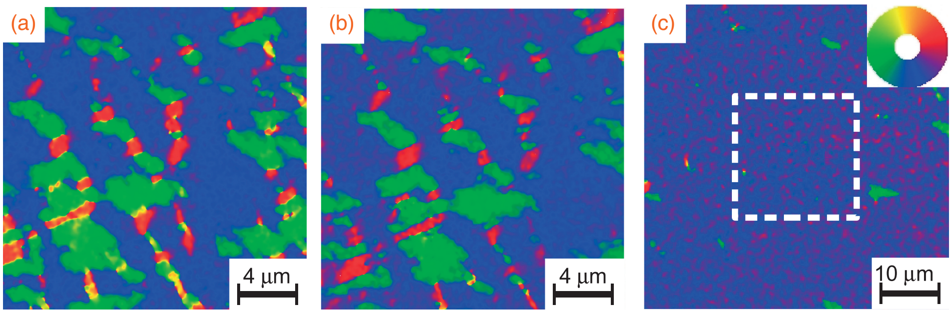

Fig. 4. Magnetic domain images of (a) 5.0 ML, (b) 8.8 ML, and (c) 21 ML Fe on the 1 L alumina samples. These images are taken at the same location on the sample. Area enclosed by the white dashed line in (c) corresponds to the same area as those in (a) and (b).

and very few yellow regions. In the sample of 8.8 ML Fe, shown in Fig. 4(b), the yellow domains almost disappear, and the green and red areas decrease slightly. In this case, the Fe on the alumina should already be in the ferromagnetic phase. Because its Curie temperature is around room temperature, however, the magnetization is still weak, and no crucial influence on the domains can be observed. However, if the Fe coverage is increased to 21 ML, the domain becomes so large that the entire field of view becomes a blue area. The zoomed-out image in Fig. 4(c) shows that only very few green areas exist. The rotation of the small domains to the larger one as the Fe coverage increases indicates that the Fe nanoparticles on the alumina are so large and interconnected that they become ferromagnetic and merge with the domains of the neighboring Fe films. Exchange interaction causes the system to become a single domain.

From the SEMPA domain images, it is clear that the domain fragmentation of the ultrathin Fe film results from the existence of paramagnetic nanoparticles, which separate the microfilms. These microfilms seem to have magnetization along their own easy axes and form a closed domain structure between neighbors. Many domain boundaries are hence created. Such a domain pattern is not favored in a continuous film because the creation of each domain boundary requires a domain wall energy that is proportional to $\sqrt{AK}$, where A is the exchange constant, and K is the anisotropy constant.24) With so many domain walls, the free energy of the system will be raised by much more than the magnetostatic energy is reduced. Because the microfilms are separated by paramagnetic nanoparticles, the creation of domain boundaries requires much less energy and can further reduce the magnetostatic energy. Therefore, one paramagnetic nanoparticle chain can be effective in separating the magnetic domains.

In conclusion, instead of the large magnetic domains in a continuous ultrathin film, ultrathin Fe deposited on alumina nanopatterns reveals a fragmented magnetic domain structure on the nanoscale. The paramagnetic nanoparticle chains are effective in partitioning the magnetic domains and re-aligning the domain direction. These microfilms tend to have magnetization along their own easy axes and form a closed domain structure between neighbors so as to reduce the magnetostatic energy. This type of variation in the growth modes and Curie temperatures can be applied to other surfaces that have nanosized heterostructures formed either by self-assembly or lithography techniques. This might provide another approach to implementing bit-patterned storage media for application in information technology.

Acknowledgment This work was supported by the National Science Council of Taiwan under Grant Nos. NSC 96-2120-M-002-011, NSC 95-2112-M-002-051-MY3, NSC 96-2112-M-003-015-MY3, and NSC 102-2112-M-033-004-MY3. A portion of this research was conducted at the Center for Nanophase Materials Sciences, which is a DOE Office of Science User Facility.

---

1) J. Martín, J. Nogués, K. Liu, J. Vicent, and I. K. Schuller, J. Magn. Magn. Mater. **256**, 449 (2003).
2) T. R. Albrecht, D. Bedau, E. Dobisz, H. Gao, M. Grobis, O. Hellwig, D. Kercher, J. Lille, E. Marinero, K. Patel, R. Ruiz, M. E. Schabes, L. Wan, D. Weller, and T.-W. Wu, IEEE Trans. Magn. **49**, 773 (2013).
3) J. M. De Teresa and A. Fernández-Pacheco, Appl. Phys. A **117**, 1645 (2014).
4) B. D. Terris and T. Thomson, J. Phys. D **38**, R199 (2005).
5) J. C. Lodder, *Advanced Magnetic Nanostructures* (Springer, New York, 2006).
6) B. Aktas, L. Tagirov, and F. Mikailov, *Magnetic Nanostructures* (Springer, Heidelberg, 2007).
7) M. Bode, O. Pietzsch, A. Kubetzka, and R. Wiesendanger, Phys. Rev. Lett. **92**, 067201 (2004).
8) S. Rusponi, N. Weiss, T. Cren, M. Epple, and H. Brune, Appl. Phys. Lett. **87**, 162514 (2005).
9) H.-J. Freund, Surf. Sci. **500**, 271 (2002).
10) J. P. Pierce, M. A. Torija, Z. Gai, J. Shi, T. C. Schulthess, G. A. Farnan, J. F. Wendelken, E. W. Plummer, and J. Shen, Phys. Rev. Lett. **92**, 237201 (2004).
11) J. Brandenburg, R. Hühne, L. Schultz, and V. Neu, Phys. Rev. B **79**, 054429 (2009).
12) M. Dreyer, M. Kleiber, A. Wadas, and R. Wiesendanger, Phys. Rev. B **59**, 4273 (1999).
13) R. P. Blum, D. Ahlbehrendt, and H. Niehus, Surf. Sci. **396**, 176 (1998).
14) N. Frémy, V. Maurice, and P. Marcus, J. Am. Ceram. Soc. **86**, 669 (2003).
15) P. J. Hsu, C. B. Wu, H. Y. Yen, S. S. Wong, W. C. Lin, and M. T. Lin, Appl. Phys. Lett. **93**, 143104 (2008).
16) W. C. Lin, C. C. Kuo, M. F. Luo, K. J. Song, and M. T. Lin, Appl. Phys. Lett. **86**, 043105 (2005).
17) W. C. Lin, P. C. Huang, K. J. Song, and M. T. Lin, Appl. Phys. Lett. **88**, 153117 (2006).
18) C. A. F. Vaz, J. A. C. Bland, and G. Lauhoff, Rep. Prog. Phys. **71**, 056501 (2008).
19) W. C. Lin, S. S. Wong, P. C. Huang, C. B. Wu, B. R. Xu, C. T. Chiang, H. Y. Yen, and M. T. Lin, Appl. Phys. Lett. **89**, 153111 (2006).
20) M. Stampanoni, A. Vaterlaus, M. Aeschlimann, and F. Meier, Phys. Rev. Lett. **59**, 2483 (1987).
21) M. T. Lin, W. C. Lin, C. C. Kuo, and C. L. Chiu, Phys. Rev. B **62**, 14268 (2000).
22) R. P. Blum, H. Niehus, and D. Ahlbehrendt, Surf. Sci. **366**, 107 (1996).
23) W. C. Lin, Z. Gai, L. Gao, J. Shen, P. J. Hsu, H. Y. Yen, and M. T. Lin, Phys. Rev. B **80**, 024407 (2009).
24) B. D. Cullity, *Introduction to Magnetic Materials* (Addison-Wesley, Reading, MA, 1972).